



Noble gases and rock geochemistry of alkaline intraplate volcanics from the Amik and Ceyhan-Osmaniye areas, SE Turkey.



F. Italiano^{a,*}, G. Yuçe^b, M. Di Bella^{a,c}, B. Rojay^d, G. Sabatino^c, A. Tripodo^c, M. Martelli^a, A.L. Rizzo^a, M. Misseri^a

^a Istituto Nazionale di Geofisica e Vulcanologia Sezione di Palermo, Via Ugo La Malfa, 153, 90146 Palermo, Italy

^b Hacettepe University, Department of Geological Engineering, Beytepe, 06800, Ankara, Turkey

^c University of Messina, Department of Mathematics and Computer Sciences, Physic Sciences and Earth Sciences, Viale G. d'Alcontres, 31, 98166 S. Agata, Messina, Italy

^d Middle East Technical University, Department of Geological Engineering, 06531 Ankara, Turkey

ARTICLE INFO

Keywords:

Transtensional Amik Basin
Toprakkale volcanic province
Noble gases
Fluid inclusions
Trace elements
Turkey

ABSTRACT

The SE part of Turkey is characterized by a transtensional regime within the complex collision zone between the Anatolian, Arabian and African plates, which is bounded by two main faults, Dead Sea Fault and its splays on east and the Karasu Fault on west. In this tectonic and geodynamic context developed the Amik and further North, Erzincan and Toprakkale districts, which are located onshore the Iskenderun Gulf, with the occurrence of a widespread and young alkaline volcanism dated from 1.57 to 0.05 Ma in Amik, and 2.25 to 0.61 Ma in Toprakkale.

Here we present the results of a petrochemical and noble gases (He–Ar) study performed in basalts and basanites from the Basins in order to constrain the features of the mantle source. The major and trace elements composition indicate that the involved mafic melts could be the result of 0.8–2% partial melting of a predominantly spinel and garnet + spinel mantle, which has typical features of intra-plate OIB magmatism. The $^4\text{He}/^{40}\text{Ar}^*$ ratios display two distinct ranges, roughly < 1 and > 1 , for basalts and basanites respectively. The $^3\text{He}/^4\text{He}$ ratio of fluid inclusions in olivine crystals ranges from 7.29 to 8.03 Ra (being Ra the atmospheric $^3\text{He}/^4\text{He}$ ratio of 1.39×10^{-6}), which implies a rather homogenous helium isotope signature of the mantle source. Such values are commonly recorded in MORB-like reservoirs (namely 8 ± 1 Ra), confirming that lavas erupted in SE Turkey did not suffer any important process of crustal contamination.

Combining the main evidences from the geochemical data of both rocks and noble gases of fluids inclusions, we suggest that the melt generation of the alkaline magmas was triggered by a stretching lithosphere resulting from asthenosphere upwelling and decompression melting, analogous to geodynamic models of the coeval Syrian alkaline volcanic rocks and the older NW Anatolian rocks, rather than by subduction or plume-related processes. Finally, the combined results of noble gas-rock geochemistry point to a widespread mantle metasomatism as well as absence of crustal assimilation and negligible crustal contamination in contrast to former conclusions based only on the solid rock geochemistry.

1. Introduction

Collision tectonics along Bitlis-Zagros thrust belt is ended with the evolution of strike slip tectonics in SE Anatolian, namely, the evolution of Dead Sea (DSF) and Eastern Anatolian Faults (EAF) (Fig. 1). Two peculiar areas are the Amik Basin within Karasu Rift and Toprakkale Volcanic Field to the north of Iskenderun Basin (Fig. 1). The neotectonic structure in the Amik Basin (SE Turkey) formed in a transtensional setting under the control of DSF strike slip faults within the collision zone of the African and Arabian plates with the Eurasian plate in SE

Anatolia since the Plio-Quaternary (since 5.4 Ma) (Fig. 1; Barka and Reilinger, 1997; Hempton, 1987; Gürsoy et al., 2003). The Amik area is characterized by the widespread presence of basalt outcrops either as small volcanic edifices or from fissure eruptions within Karasu Rift having a 1.6 km thick sedimentary package on the top an ophiolite (Turkish Petroleum TPAO Amik-1 well records done in 1987) along the continuation of the DSF. In the Toprakkale area, the basaltic volcanism is located just to the northern coast of the Iskenderun Basin along Karataş-Osmaniye Fault (KOF). However, none of the outcrops exhibits any active gas emissions.

* Corresponding author.

E-mail address: francesco.italiano@ingv.it (F. Italiano).

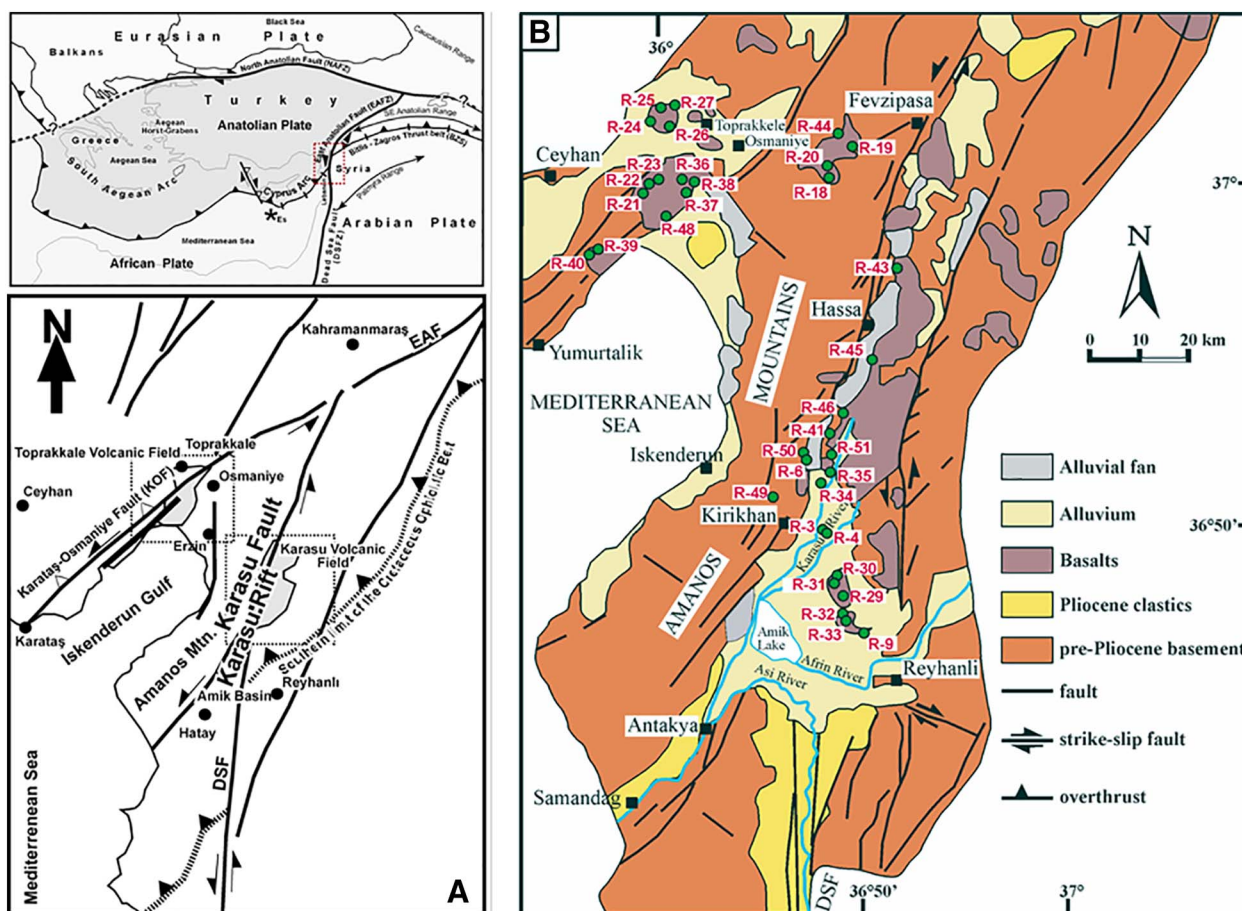


Fig. 1. (a) Sketch map of the study area in the main frame of the three tectonic plates Anatolian, Arabian, African plate (on the top) and the location of the Amik and the Iskenderun Basins (bottom) (modified from Bağcı et al., 2011); (b) Location of the sampled rocks in the simplified geological map of the Amik (Hatay) and Erzin (Ceyhan-Osmaniye) areas (modified from Bağcı et al., 2011).

Recent investigations carried out over the Amik Basin, highlighted a diffuse degassing of mantle-derived volatiles mainly composed by CO_2 with helium isotope ratios in the range of 0.8–1.7Ra (Yuçe et al., 2014). The presence of a diffuse mantle contribution to the fluids (bubbling gases and gases dissolved in cold and thermal waters) was recorded all over the Amik Basin, from the southern branch of the Karasu Fault to the West, up to the its junction with the EAF to the North, and across the plates boundary that is the active, strike-slip DSF to the East and South (Fig. 1). The widespread presence of CO_2 testifies a regional degassing activity interpreted to be likely related to the DSF rather than to volcanic degassing (Yuçe et al., 2014). Moreover, the serpentinization process responsible for the production of abiogenic methane and hydrogen is not related to mantle-type contribution, although the helium isotope ratio always indicated variable contents of mantle-derived fluids (Yuçe et al., 2014). Indeed, $^3\text{He}/^4\text{He}$ of up to 1.71 Ra in the Amik Basin are not consistent with the presence of recent eruptive activity, but it can only be related to the degassing activity of the active faults crossing the Amik Basin (Yuçe et al., 2014).

The volcanism over the study areas includes tholeiitic and alkaline olivine basaltic eruptions. Several petrologic studies interpreted the intracontinental volcanism and the genetic relationships between alkaline and sub-alkaline magmas besides the nature of mantle sources feeding the various volcanic centers. The “Karasu Rift” hosts both tholeiitic and alkaline basalts interpreted as derived from an OIB-like source (Alici et al., 2001) with the tholeiitic basalts contaminated by some crustal assimilation (Polat et al., 1997). Polat et al. (1997) and Parlak et al. (1997, 1998) proposed that alkali olivine basalts derived from an asthenospheric mantle source, following the lithospheric fractures of the strike-slip DSF and the EAF in southern Turkey.

Yurtmen et al. (2002) suggested that some groups of basalts resemble extension-related alkali basalts; others are similar to ocean island basalts or show subduction-related characteristics. On the other hand, it is proposed that the Plio-Quaternary basic volcanism, originated from different degree of partial melting of an isotopically depleted mantle source, is related to decompressional melting under a transtensional tectonic regime in Ceyhan-Osmaniye area (Parlak et al., 2000; Yurtmen et al., 2000; Bağcı et al., 2011).

Several studies using K–Ar determinations suggest that the volcanism is younger than 2.25 Ma, in a range of 2.25 to 0.06 Ma (Çapan et al., 1987; Yürür and Chorowicz, 1998; Arger et al., 2000; Alici et al., 2001; Rojay et al., 2001; Yurtmen et al., 2002), where there was intermittent volcanism during 1.73 Ma–0.08 Ma (Rojay et al., 2001).

This paper provides new and original information using the combined results of noble gases geochemistry and petro-geochemical analyses carried out on rocky samples collected from the scattered volcanic outcrops occurring along the extensional Amik Basin. The study is based on the analyses of noble gas (He–Ar isotopes) in fluid inclusions from olivines as well as the major and trace elements determinations of the volcanics.

2. Tectonic setting of the area

The geodynamics of Eastern Mediterranean is the result of relative motion between Eurasian, African and Arabian plates (e.g., Şengör et al., 1985; Barka and Reilinger, 1997; Reilinger et al., 1997; McClusky et al., 2000) with several episodes of magmatic activity linked to the tectonic evolution since Late Cretaceous.

Following the sea floor spreading, Arabian plate was rifted away

from Africa along the Red Sea. During the Middle to the Late Miocene, the subducting edge of northern border of Arabian plate collided with the southern margin of Eurasian plate along the Bitlis-Zagros Thrust Zone. In time, Dead Sea Fault (DSF) propagates to the North, a part of the Eurasian lithosphere (Anatolian Plate), shortened and thickened, then started to move westwards toward the Hellenic subduction zone where the northern African oceanic slab is underplated. The lateral extrusion of this lithospheric mass, represented as the Anatolian Plate, is accommodated by two transform faults, namely, the North Anatolian Fault (NAF) and the East Anatolian Fault (EAF) (Şengör et al., 1985; Kiritzi, 1993; Barka and Reilinger, 1997; Yürür and Chorowicz, 1998). The EAF is linked with propagating DSF during 5.4 Ma (Hempton, 1987).

Within that tectonic frame, various structure-controlled basins with volcanic fields are developed, such as Iskenderun and Amik Basins. The 2.25 to 0.61 Ma age (Arger et al., 2000) Toprakkale volcanic field is located along the sinistral strike slip Karatas-Osmaniye Fault (KOF), which borders the Iskenderun Basin developed on top of imbricated ophiolitic suites that are the continuity of Cyprus imbricated mass with crustal fragments (Amanos Mountains). The Amik Basin is the southern part of the Karasu Rift and is located along the intersection domain of several regional-scale structural lineaments, namely the N trending sinistral DSF, the NE trending sinistral EAF and the NE trending contractional Cyprus Arc (CA) (Fig. 1). The basin, where most of the samples have been collected, is an asymmetrical composite transtensional basin developed between the seismically active left-lateral DSF splays and the left-lateral oblique-slip Karasu Fault during neotectonic period (Muehlberger, 1981). The Iskenderun basin (where Toprakkale volcanic field developed) is located to the West of Amanos High and Amik Basin (where Karasu volcanic field developed) to the East of the Amanos High. Both basins are located within or near the triple junction that is developed between Arabian Plate, African Plate and Anatolian Block (Barka and Reilinger, 1997; Meghraoui et al., 2011; Mahmoud et al., 2013).

3. Analytical methods

Thirty-three samples were collected from fresh and massive lava flows of the volcanic outcrops from Amik (Hatay) and Erzincan (Ceyhan-Osmaniye) (Table 1).

In the field the blocks were broken by a heavy hammer in order to verify the integrity of the rock matrix (absence of alterations and scoria). The samples have been then moved to the laboratories for the analytical measurements following the procedures detailed below.

3.1. Mineralogical-geochemical methods

The main mineral phases were analysed at Messina University by SEM-EDS using a FEI Inspect instrument, coupled with an Oxford INCA PentaFETx3 EDX spectrometer, Si(Li) detector, nitrogen cooled, equipped with an ultra-thin window ATW2, with a resolution of 137 eV at 5.9 keV (Mn-K α 1). Some representative SEM images of Fig. 2(A–F) show morphological features of olivine and clinopyroxene crystals.

The spectral data were acquired at a working distance of 10 mm with an acceleration voltage of 20 kV, counting times of 60 s, with approximately 3000 counts/s (cps). The quality control of the analyses was made on Corning “Glass Type A”. The results were processed by the INCA software Energy, based on the XPP matrix correction scheme developed by Pouchou and Pichoir (1984, 1985).

Major (SiO₂, TiO₂, Al₂O₃, FeO_{tot}, MnO, CaO, K₂O, P₂O₅; Table 2) elements of all samples and some trace elements of samples R41–R51 (Co, Cr, Ni, V, Sc, Ba, Cs, Ga, Sr, Rb, U, Zr, Nb, Y, Pb, Th, La, Ce; Table 3) were carried out at the Messina University laboratories by X-ray fluorescence using a wavelength-dispersive automated Philips PW 1400 spectrometer on powder pellets produced by milling the rocks in a

Table 1

List of the collected samples from the Amik and Toprakkale volcanic areas. The list includes the rock type, the areas/village name and the samples location in coordinates expressed in WGS84 units. n.d. = not determined.

Sample ID	Rock type	Latitude	Longitude	Site
Amik basin				
R-18	Basalt	37.05389	36.63389	Islahiye town
R-19	Basalt	37.08583	36.64167	Islahiye town
R-20	Basalt	37.06722	36.63167	Islahiye town
R-29	Basalt	36.42833	36.54250	Reyhanli-Hamamat
R-30	Basalt	36.43556	36.54611	Reyhanli-Hamamat
R-31	Basalt	36.42806	36.54083	Reyhanli-Hamamat
R-32	Basalt	36.41056	36.54111	Reyhanli-Hamamat
R-33	Basalt	36.41361	36.54083	Reyhanli-Hamamat
R-34	Basalt	36.57500	36.55278	Yalangoz town
R-35	Basalt	36.57167	36.53000	Yalangoz town
R 41	Basalt	36.94681	36.58013	Bogazici
R 43	Basalt	36.87699	36.59197	Ciftegoz
R 44	Basalt	37.08848	36.63778	Armutlu - Fevzipasa well
R 45	Basalt	36.75172	36.49234	On the road to Hacilar
R 46	Basalt	36.66794	36.49844	Akkuler
R 49	Basalt	36.56445	36.38698	Ceylanli
R 50	Basalt	36.57387	36.50174	In proximity to Yalangoz
R 51	Basalt	36.57950	36.53363	Incirli
Toprakkale volcanic district				
R-21	Basanite	37.01306	36.06889	Delihalil (volcanic chimney)
R-22	Basanite	37.04000	36.09500	Delihalil (volcanic chimney)
R-23	Basanite	37.03861	36.08611	Delihalil (volcanic chimney)
R-24	Basalt	37.11167	36.08250	Uctepe (volcanic chimney)
R-25	Basanite	37.11944	36.09083	Uctepe (volcanic chimney)
R-26	Basanite	37.11889	36.09722	Uctepe (volcanic chimney)
R-27	Basalt	37.10944	36.05694	Uctepe (volcanic chimney)
R-28	Basanite	37.11944	36.09083	Uctepe (volcanic chimney)
R-36	Basanite	37.04417	36.13194	Toprakkale town
R-37	Basanite	37.04556	36.13083	Toprakkale town
R-38	Basanite	37.04194	36.13806	Toprakkale town
R-39	Basalt	36.89888	35.89874	Yumurtalik village
R-40	Basalt	36.90111	35.90000	Yumurtalik village
R 47	Basalt	n.d	n.d	Toprakkale
R 48	Basanite	36.98691	36.11967	Delihalil

steel jaw crusher and then in agate mortars up to a fine powder. MgO and Na₂O concentrations were determined by atomic absorption spectrophotometry and flame emission on sample solution after perchloric and hydrofluoric acid attack. FeO content was measured by titration after rapid HF-H₂SO₄ attack. LOI (Loss on Ignition) is the weight loss after heating at 950 °C. Precision is better than 5% for all elements.

Trace element analyses of samples R18–R39 (Table 3) were performed at ACME Analytical Laboratories Ltd, Vancouver, Canada by LA-ICP-MS.

3.2. Noble gas analytical methods

Ten rock samples were selected for noble gases analysis in fluid inclusions at the laboratories of Istituto Nazionale di Geofisica e Vulcanologia, Sezione di Palermo (INGV-Palermo). Given that among the main crystal phases, olivine is the best candidate to store the original magmatic signal into the fluid inclusions, the samples to be analysed have been selected on the basis of the olivine crystals availability. Bulk rocks were mechanically fragmented, sieved at a fraction size of 0.5–1 mm and treated with Na polytungstate heavy liquid for olivine separation from scoria. Crystals were then handpicked under a binocular microscope. To prevent any contamination of gas released from fluid inclusions, we only considered olivine crystals without glassy and/or altered surfaces around the crystal. An amount of 0.1–1.9 g of olivine crystals was finally loaded in a stainless-steel basket and placed in a crusher capable of loading up to six samples simultaneously. Olivine crystals were analysed for the He–Ne–Ar

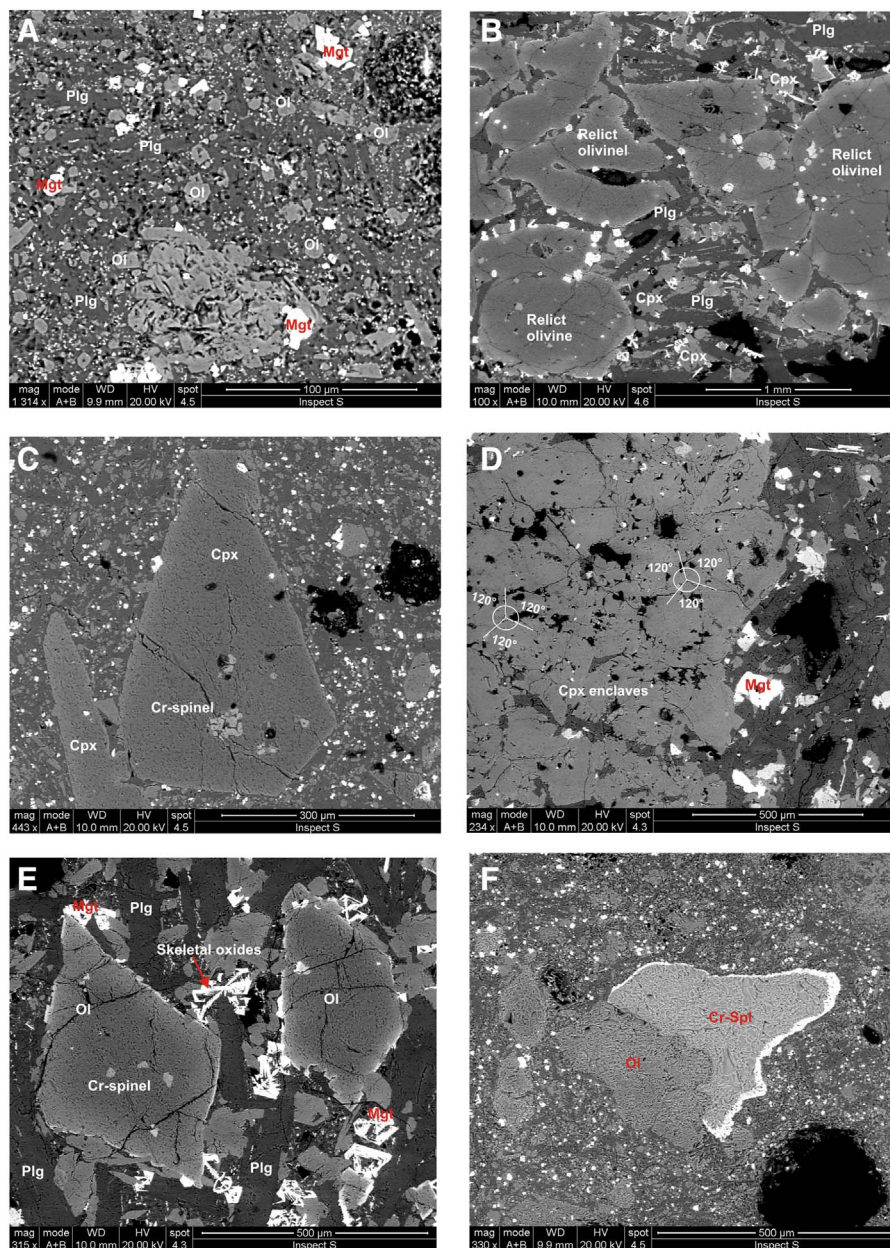


Fig. 2. SEM-BSE images of the main representative petrographic structures: A) Sample R30-basalt - small to medium sized fresh olivine phenocrysts in basanite; B) Sample R38 – basanite - medium to large sized relict olivine phenocrysts; C) Sample R25 – basanite - large clinopyroxene phenocrysts; D) Sample R44-basalt - polygonal structure of clinopyroxene enclaves; E) Sample R40-basalt olivine phenocrysts including Cr-spinel and skeletal magnetite crystals; F) Sample R25 – basanite - xenocrystic aggregates of olivine and Cr-spinel.

abundance and isotope ratio of fluid inclusions. The gas phase was extracted by single step crushing of crystals at 200 bars under ultra-high-vacuum conditions in order to prevent the release of noble gases component retained in the crystal lattice. The gas mixture was purified in a preparation line in order to remove all of the species except noble gases. He, Ne, and Ar were then separated from each other and admitted into the appropriate mass spectrometers. The He isotope composition and ^{20}Ne were determined by separately introducing the species into two different split-flight-tube mass spectrometers (both thermo-Helix SFT). The $^3\text{He}/^4\text{He}$ ratio is expressed as R/Ra (where Ra is the $^3\text{He}/^4\text{He}$ ratio of air, which is equal to 1.39×10^{-6}) and the analytical error was generally $< 1\%$ depending on the He content. The R/Ra values were corrected for atmospheric contamination based on the $^4\text{He}/^{20}\text{Ne}$ ratio (Sano & Wakita, 1985). The Ar-isotope composition was measured in a multicollector mass spectrometer (GVI-Argus), for which the analytical uncertainty was generally $< 0.5\%$. The instrumental uncertainty in the determinations of He, Ne, and Ar elemental

contents was $< 5\%$. Typical blanks for He, Ne, and Ar were $< 10^{-14}$, $< 10^{-16}$ and $< 10^{-14}$ mol, respectively. To recalculate elemental and isotope ratios of He, Ne, and Ar we purified 0.1 cc³ of air standard, which followed the same procedure above described for gas released from fluid inclusions. Further details on sample preparation and analysis procedure can be found in Martelli et al. (2014), Di Piazza et al. (2015) and Rizzo et al. (2015).

4. Results

4.1. Classification, petrography and mineral chemistry

The volcanic suite is composed of silica undersaturated rocks (Table 1), characterized by sodic affinity according to Le Maitre (2002) classification ($\text{Na}_2\text{O} - 2 > \text{K}_2\text{O}$). The total alkali versus silica diagram (Fig. 3A) evidences that they are basalts and basanites and fall in the alkaline field.

Table 2
Results of the XRF data for major oxides analysed for the studied lavas.

Sample ID	SiO ₂	Al ₂ O ₃	Fe ₂ O ₃	MgO	CaO	Na ₂ O	K ₂ O	TiO ₂	P ₂ O ₅	MnO	LOI
wt%											
R18	50.10	16.50	11.42	5.82	8.74	3.39	1.20	1.9	0.34	0.14	0.20
R19	49.90	16.66	11.54	5.89	8.58	3.54	1.40	2.09	0.41	0.14	0.10
R20	50.00	16.80	11.48	5.59	8.50	3.53	1.40	2.09	0.42	0.14	0.10
R21	45.10	15.64	11.92	8.00	8.29	4.74	2.40	2.73	0.89	0.17	0.10
R22	46.50	16.11	11.46	6.92	7.65	5.85	1.40	2.48	0.75	0.17	0.50
R23	46.20	15.78	11.43	7.63	7.82	4.95	2.40	2.48	0.73	0.16	0.20
R24	45.60	15.65	12.41	8.88	10.2	3.21	1.10	2.43	0.41	0.15	0.10
R25	44.70	14.95	11.89	9.05	9.09	4.33	2.30	2.79	0.78	0.16	0.10
R26	46.70	16.11	11.00	7.29	7.41	5.06	2.90	2.48	0.74	0.16	0.10
R27	45.50	15.61	12.50	8.80	9.97	3.5	1.20	2.50	0.44	0.15	0.10
R28	45.90	16.03	11.32	7.82	7.74	5.07	2.70	2.61	0.76	0.16	0.10
R29	49.50	16.42	11.96	6.37	9.58	3.22	0.70	1.67	0.28	0.15	0.10
R30	50.50	15.84	12.05	6.21	9.23	3.28	0.90	1.72	0.30	0.15	0.10
R31	50.20	15.78	12.03	6.48	9.44	3.25	0.90	1.72	0.30	0.15	0.10
R32	46.40	15.28	12.79	7.62	10.5	3.18	1.10	2.47	0.51	0.16	0.10
R33	46.20	15.51	12.71	7.48	10.4	3.32	1.10	2.48	0.50	0.16	0.10
R34	47.30	14.28	12.48	10.1	9.10	2.91	1.10	1.87	0.37	0.16	0.20
R35	48.90	16.17	12.22	6.11	9.17	3.47	1.30	2.11	0.46	0.16	0.10
R36	44.20	15.53	13.06	7.79	10.7	3.78	1.50	2.91	0.91	0.16	0.10
R37	44.10	15.31	13.23	7.45	10.7	3.90	1.50	2.89	0.93	0.16	0.10
R38	44.40	15.56	13.27	7.06	10.9	3.86	1.40	2.93	0.90	0.16	0.10
R40	48.1	14.92	12.70	8.73	9.82	3.28	0.70	1.78	0.42	0.16	0.10
R41	47.62	15.93	12.56	4.81	10.21	3.86	1.33	2.11	0.80	0.17	0.14
R43	47.37	16.49	13.32	3.89	10.69	3.56	1.15	2.29	0.52	0.17	0.16
R44	49.48	16.81	12.59	3.62	9.30	3.45	1.45	2.18	0.49	0.17	0.22
R45	46.93	17.43	12.31	3.63	10.93	3.44	1.46	2.34	0.79	0.17	0.14
R46	48.55	17.08	12.43	3.66	10.55	3.43	1.16	2.08	0.40	0.17	0.15
R47	48.90	17.12	12.52	4.78	9.64	3.78	0.85	1.84	0.49	0.16	0.18
R48	44.58	15.82	13.09	5.68	9.52	5.29	1.69	2.89	1.32	0.18	0.22
R49	49.44	17.02	11.32	4.12	9.19	3.77	1.41	1.93	0.54	0.17	0.19
R50	50.26	17.69	11.51	4.22	8.86	3.48	1.51	1.90	0.66	0.16	0.26
R51	49.37	16.04	12.04	5.28	9.28	3.72	1.26	1.91	0.50	0.16	0.11

Petrographic analyses show that basanites are from fine to medium grained and from moderately (phenocrysts contents around 15–20%) to highly porphyritic (30–35%). Basalts are frequently from poorly to moderately porphyritic (10–20 vol% phenocrysts) and commonly display sub-ophitic or intergranular textures. Both rock types contain from small, medium to large phenocrysts of olivine and minor clinopyroxene. The groundmass is cryptocrystalline for basanites, microcrystalline for basalts and generally made up of variable amount of plagioclase, clinopyroxene and opaque minerals (magnetite, ilmenite). Overall in basanites, xenolithic clinopyroxene aggregates with polygonal structure occur besides rare partially resorbed xenocrystic amphibole (Kaersutite; brown hornblende; e.g., R25 basanite).

Since olivine represents a key phase for the noble gas analyses in fluid inclusions, petrographic analyses were carried out of both rock types where olivine occurs in different morphologies, with euhedral and subhedral habitus (Fig. 2A), frequently displaying skeletal (quench structure) shapes indicating rapid cooling and containing magnetite inclusions. No significant compositional zoning has been observed and generally the composition ranges from Fo₇₀ to Fo₇₅. In some basalts, olivine crystals are partially or totally altered to iddingsite with alterations localized along rims and fractures. In some basanites, subordinate anhedral and subhedral olivines are found with Cr-rich spinel inclusions (Fig. 2B) and forsteritic component enrichment (Fo_{80–88}). Sometimes they are interested by low degrees of serpentinization along rims and fractures. All of these olivines display CaO content increase from the core (0.31%) to the rim (2.85%) with the subhedral crystals generally marked by higher Ca-depletion. The increase in Ca at the rims is interpreted as a response to a sudden pressure drop during magma ascend and eruption (Stormer, 1973). Furthermore, high CaO values suggest crystallization in a shallow environment.

Large sized clinopyroxene phenocrysts (Fig. 2C) occur in basanites

and are characterized by anhedral, frequently fractured habitus of salitic composition.

Plagioclase phenocrysts occur only in some basalts with labradoritic and andesinic composition. Microlites of groundmass show andesinic, oligoclasic up to anorthoclastic compositions. Only on very rare occasions, sanidine laths are encountered in the groundmass of some basalt samples.

Apart for the phenocrysts present, a crystallization sequence in the groundmass passing from olivine (rare) through clinopyroxene, Ti–Fe oxides, nepheline, plagioclase and finally to glass. Groundmass Fe–Ti oxides are mainly titanomagnetite and ilmenite. In many samples, they show a skeletal texture (Fig. 2E). Spinel included in clinopyroxene and olivine phenocrysts range from Cr-spinel (Cr# up to 65.6 mol%; Fig. 2C and Fig. 2E) to titanomagnetite-spinel (up to 3 + 68.5 mol% MgFe₂O₄ component; Fig. 2).

4.2. Major and trace element composition

The bulk-rock major- and trace-element compositions of the Pleistocene-Quaternary volcanic rocks from the Amik Basin and Ceyhan-Osmaniye area are provided in Tables 2 and 3. Basanites and alkali basalts exhibit different bulk rock compositions. The most important feature is represented by the general enrichment in incompatible trace elements showed by the Si-undersaturated basanites to the respect of the alkali basalts (Fig. 3). The major oxides display a sharp increase in Fe₂O₃, CaO and Cr₂O₃ with increasing MgO besides constant Na₂O, K₂O and P₂O₅ contents.

All basanites and four alkali basalts from Toprakkale-Erzin and Reyhanli-Amik (R24, R27, R32, R33) show the highest TiO₂ values (> 2.43 wt%; Table 2) as a consequence of the high amount of opaque phases and Ti-augites groundmass grains. Overall, the major elements trends suggest an evolution through a low degree of fractional crystal-

Table 3
Results of the LA-ICP-MS and XRF (^a) trace elements data analysed for the studied lavas.

Sample ID	Cr	Ni	Sc	Ba	Co	Cs	Ga	Hf	Nb	Rb	Sr	Ta	Th	U	V	Zr	Y	Pb
ppm																		
R18	150	36	23	244.5	43.3	0.1	20.8	3.8	21.2	22.8	494.4	1.2	3.3	0.8	197	146.6	24	1.6
R19	120	30	23	320.2	42.8	< 0.1	22.1	4.6	28.8	20.3	542.9	1.7	5.1	0.4	219	178.5	27.6	3.8
R20	130	26	23	307.9	40.8	< 0.1	21.1	4.3	27	19.1	533.4	1.5	3.5	0.4	214	167.5	27.2	3.8
R21	190	106	19	303.7	48.3	0.4	21.9	6.8	58.7	30.1	900.0	3.7	6.2	1.7	192	298.4	29.3	2.0
R22	130	103	18	344.4	46.3	0.5	23.9	8.0	71.8	26.3	991.9	4.7	8.3	2.2	179	363.9	31.7	3.2
R23	170	109	20	356.7	50.8	0.3	23.6	7.4	65.5	34.7	912.5	4.2	8.5	2	189	333.4	29.9	2.0
R24	280	132	25	206.2	55.3	< 0.1	20.6	3.6	26.1	9.0	712.5	1.4	3.3	0.7	243	134.1	23.1	1.6
R25	280	186	20	289.3	53.3	< 0.1	20.3	5.4	52.4	24.7	917.1	3.2	4.9	1.4	219	253.2	26.3	2.9
R26	160	120	17	299.5	54.1	0.5	22.9	8.4	63.8	35.1	906.3	4.3	6.8	2.2	176	336.3	29.9	3.7
R27	260	136	25	201.2	56.9	< 0.1	19.3	3.4	25.8	10.5	695.2	1.6	2.7	0.7	241	134.9	23.7	1.7
R28	190	134	18	285.2	49.9	0.2	21.1	6.5	55.7	28.9	846.6	3.8	4.7	1.7	184	291.1	25.5	0.9
R29	280	39	24	221.3	46.5	0.3	21.8	3.2	14.7	10.7	442	1.0	2.8	0.6	217	114	23.8	1.7
R30	300	47	24	271.7	45.4	0.3	24.0	3.6	16.5	21	443.9	1.0	3.1	0.7	235	128.9	27	2.4
R31	270	40	24	229.0	47.6	0.2	22.9	3.4	16.1	17.7	453.3	1.1	2.3	0.6	236	123.4	26.7	2.1
R32	230	118	25	387.9	48.8	< 0.1	21.3	3.5	32.3	14.7	621.4	2.0	2.8	0.7	227	132	22.7	2.0
R33	240	103	25	288.2	49.1	< 0.1	21.7	3.7	32.6	14.7	614.7	1.9	2.7	0.6	220	132.9	21.9	1.9
R34	430	215	25	296.9	61.1	0.3	21.7	4.0	24.1	21.1	502.2	1.6	3.8	0.9	208	134.6	23.8	1.7
R35	150	60	24	269.6	45.8	< 0.1	22.6	4.2	27.4	26.2	544.3	1.6	3.3	0.5	218	150.1	25.9	2.2
R36	200	81	25	340.8	55.4	0.1	23.6	4.3	49.6	16.2	992.1	2.6	2.7	0.9	250	184.9	28.2	1.3
R-37	190	90	25	320.8	50.6	0.1	22.9	4.1	47.7	15.7	989.6	2.6	3.4	0.9	239	179.1	27.9	1.2
R-38	170	80	25	319.5	48.7	0.1	22.8	4.2	48.1	15.4	975.2	2.5	2.8	0.9	247	181.4	28.2	1.1
R40	410	155	22	202.9	53.2	0.1	19.3	2.7	20.5	9.1	531.1	1.2	4.5	0.9	198	112.3	20.5	0.6
R41 ^a	317	156	19	246.0	34.0	24.0	22.0	n.d.	36.0	18.0	710.0	n.d.	n.d.	11.0	172	166.0	21.0	5.0
R43 ^a	220	104	21	185.0	27.0	27.0	22.0	n.d.	20.0	14.0	521.0	n.d.	n.d.	9.0	193	125.0	20.0	5.0
R44 ^a	110	33	19	264.0	25.0	24.0	24.0	n.d.	25.0	16.0	496.0	n.d.	n.d.	9.0	193	168.0	24.0	5.0
R45 ^a	127	44	20	330.0	23.0	27.0	23.0	n.d.	34.0	13.0	801.0	n.d.	n.d.	12.0	184	172.0	23.0	6.0
R46 ^a	215	85	20	217.0	28.0	24.0	23.0	n.d.	20.0	16.0	446.0	n.d.	n.d.	8.0	174	117.0	20.0	5.0
R47 ^a	263	112	18	193.0	34.0	22.0	22.0	n.d.	16.0	8.0	504.0	n.d.	n.d.	9.0	161	108.0	19.0	6.0
R48 ^a	196	154	19	325.0	34.0	33.0	23.0	n.d.	58.0	22.0	1031.0	n.d.	n.d.	14.0	197	248.0	23.0	3.0
R49 ^a	179	82	20	263.0	28.0	22.0	23.0	n.d.	20.0	19.0	456.0	n.d.	n.d.	8.0	166	135.0	25.0	8.0
R50 ^a	103	47	21	292.0	26.0	22.0	24.0	n.d.	25.0	27.0	517.0	n.d.	n.d.	9.0	174	156.0	24.0	7.0
R51 ^a	352	151	23	385.0	36.0	22.0	22.0	n.d.	22.0	19.0	467.0	n.d.	n.d.	9.0	185	138.0	23.0	7.0

Sample ID	La	Ce	Pr	Nd	Sm	Eu	Gd	Tb	Dy	Ho	Er	Tm	Yb	Lu	Pb
ppm															
R18	19.9	43.1	5.31	21.6	5.2	1.69	4.94	0.78	4.36	0.87	2.19	0.33	2.16	0.30	1.6
R19	26.8	57.8	6.86	27.5	6.2	1.97	5.84	0.92	5.11	1.03	2.56	0.38	2.3	0.36	3.8
R20	25.8	54.0	6.46	25.7	6.1	1.82	5.39	0.89	4.53	0.94	2.47	0.38	2.19	0.32	3.8
R21	41.5	86.4	9.93	39.7	7.9	2.67	7.15	1.00	5.36	1.03	2.70	0.37	2.36	0.36	2.0
R22	51.7	102.5	10.78	39.6	8.2	2.69	6.74	1.12	5.23	1.07	2.66	0.41	2.63	0.39	3.2
R23	46.2	92.5	9.86	36.8	7.6	2.54	6.25	0.99	5.17	1.05	2.63	0.41	2.65	0.38	2.0
R24	25.3	51.9	6.17	26.2	5.7	1.90	4.92	0.83	4.33	0.81	2.25	0.29	1.74	0.29	1.6
R25	40.1	81.6	8.88	37.7	7.1	2.40	6.20	0.97	4.66	0.91	2.25	0.33	2.26	0.31	2.9
R26	43.2	85.9	9.64	38.6	7.2	2.44	6.16	0.99	5.19	1.01	2.64	0.38	2.41	0.36	3.7
R27	26.2	54.4	6.54	26.6	5.8	2.00	5.18	0.81	4.54	0.86	2.25	0.32	2.02	0.27	1.7
R28	40.6	81.5	8.89	35.4	7.2	2.27	6.02	0.93	4.55	0.90	2.38	0.35	2.26	0.32	0.9
R29	18.9	38.7	4.41	19.9	4.1	1.41	4.64	0.77	4.26	0.79	2.29	0.29	2.08	0.28	1.7
R30	20.5	42.9	4.93	22.4	4.8	1.62	5.11	0.81	4.73	0.90	2.53	0.36	2.37	0.32	2.4
R31	21.6	42.4	5.04	23.2	4.8	1.66	5.37	0.84	4.76	0.91	2.49	0.32	2.22	0.34	2.1
R32	24.0	48.4	5.84	24.3	5.4	1.95	4.80	0.85	4.16	0.75	1.97	0.27	1.61	0.22	2.0
R33	23.6	48.0	5.67	24.3	5.4	1.94	4.91	0.86	4.10	0.75	1.97	0.29	1.82	0.26	1.9
R34	22.1	43.5	5.06	21.7	5.0	1.68	4.72	0.86	4.12	0.84	2.17	0.3	1.84	0.27	1.7
R35	21.6	45.1	5.49	23.4	5.7	1.89	5.24	0.92	4.65	0.88	2.43	0.36	2.02	0.31	2.2
R-36	39.1	83.7	9.49	39.4	8.1	2.74	6.97	1.04	5.45	0.99	2.36	0.34	2.22	0.27	1.3
R37	38.4	81.4	9.28	37.9	7.9	2.72	6.97	1.00	5.17	1.02	2.35	0.37	2.09	0.30	1.2
R38	38.4	82.4	9.40	38.7	8.3	2.82	6.99	1.04	5.29	1.04	2.37	0.36	1.96	0.28	1.1
R40	30.2	59.9	6.31	25.5	5.1	1.72	4.55	0.74	3.72	0.74	1.91	0.26	1.75	0.23	0.6
R41 ^a	24.0	70.0	n.d.	n.d.	n.d.	n.d.	n.d.	n.d.	n.d.	n.d.	n.d.	n.d.	n.d.	n.d.	5.0
R43 ^a	12.0	42.0	n.d.	n.d.	n.d.	n.d.	n.d.	n.d.	n.d.	n.d.	n.d.	n.d.	n.d.	n.d.	5.0
R44 ^a	17.0	62.0	n.d.	n.d.	n.d.	n.d.	n.d.	n.d.	n.d.	n.d.	n.d.	n.d.	n.d.	n.d.	5.0
R45 ^a	32.0	73.0	n.d.	n.d.	n.d.	n.d.	n.d.	n.d.	n.d.	n.d.	n.d.	n.d.	n.d.	n.d.	6.0
R46 ^a	12.0	34.0	n.d.	n.d.	n.d.	n.d.	n.d.	n.d.	n.d.	n.d.	n.d.	n.d.	n.d.	n.d.	5.0
R47 ^a	12.0	36.0	n.d.	n.d.	n.d.	n.d.	n.d.	n.d.	n.d.	n.d.	n.d.	n.d.	n.d.	n.d.	6.0
R48 ^a	45.0	112.0	n.d.	n.d.	n.d.	n.d.	n.d.	n.d.	n.d.	n.d.	n.d.	n.d.	n.d.	n.d.	3.0
R49 ^a	17.0	42.0	n.d.	n.d.	n.d.	n.d.	n.d.	n.d.	n.d.	n.d.	n.d.	n.d.	n.d.	n.d.	8.0
R50 ^a	14.0	46.0	n.d.	n.d.	n.d.	n.d.	n.d.	n.d.	n.d.	n.d.	n.d.	n.d.	n.d.	n.d.	7.0
R51 ^a	20.0	42.0	n.d.	n.d.	n.d.	n.d.	n.d.	n.d.	n.d.	n.d.	n.d.	n.d.	n.d.	n.d.	7.0

^a Samples analysed through XRF; nd – not determined.

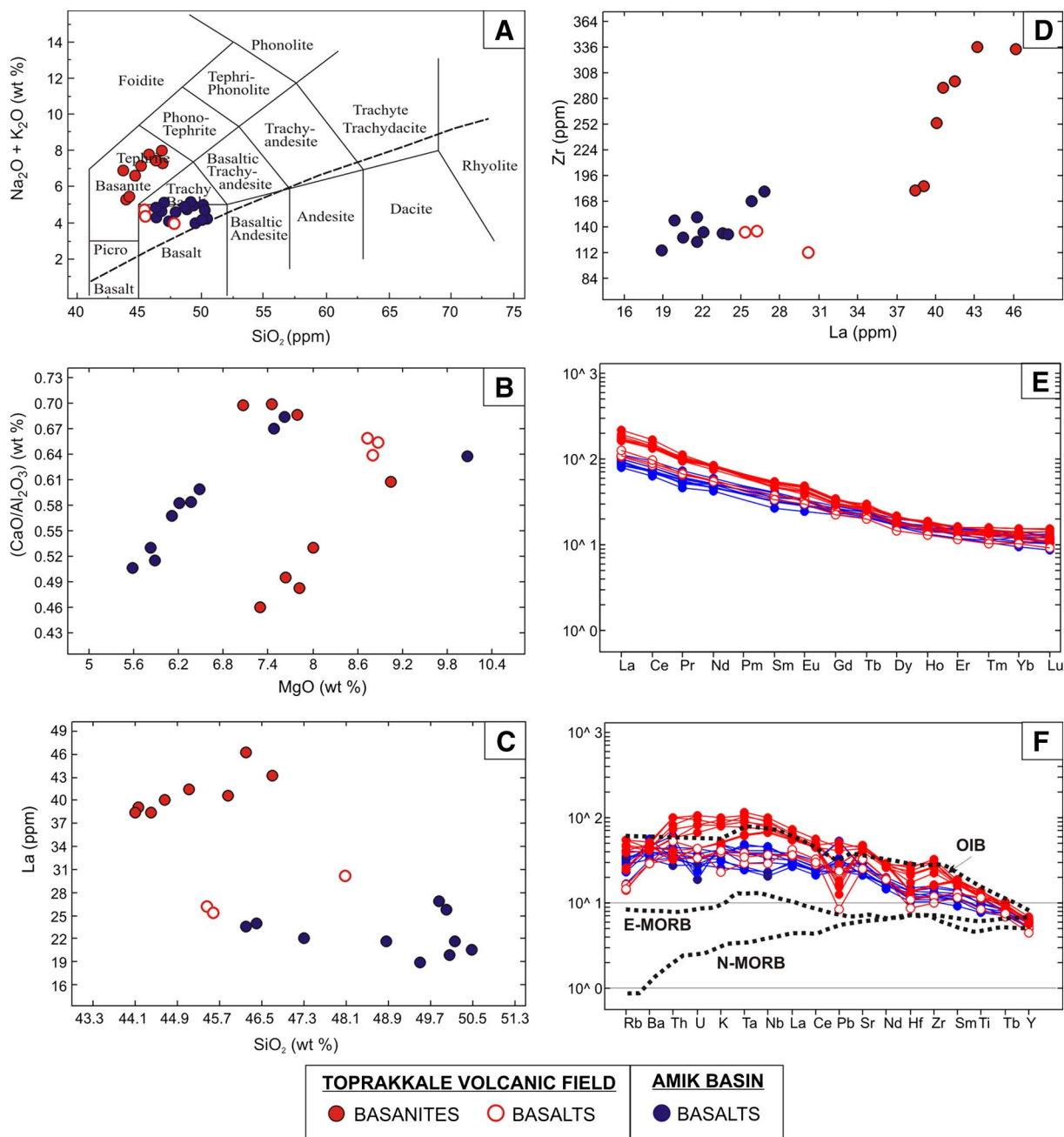


Fig. 3. A) Total Alkali vs Silica diagram, B) MgO vs CaO/Al₂O₃, C) SiO₂ vs La and D) La vs Zr variation diagrams; E) REE pattern (normalized to Chondrite Boynton, 1985); F) incompatible trace element spider diagram for the studied samples (normalized to Primordial Mantle of McDonough et al., 1992). OIB, E-MORB and N-MORB patterns after Sun and McDonough (1989). Red dots: Basanites, Blue dots: alkaline Basalts. (For interpretation of the references to colour in this figure legend, the reader is referred to the web version of this article.)

lization, dominated by olivine and clinopyroxene separation. A role of clinopyroxene fractionation is indicated by a CaO/Al₂O₃ ratio decrease with decreasing MgO (Fig. 3B).

Absolute REE ratios and abundances in basanites are higher than in alkali basalts and they generally decrease with increasing SiO₂ content (Fig. 3C). In contrast, other incompatible element ratios such as Th/Ta and Zr/Nb are almost variable in the analysed rocks. Plots of pairs of incompatible elements (Fig. 3D) define smooth trends in the basaltic compositions.

Chondrite-normalized REE patterns (Fig. 3E) show variable fractionation with La/Yb ratio from 8 to 20. The rocks display almost straight and sub-parallel chondrite-normalized REE patterns (Boynton, 1985) with nearly constant concentration ratios. Basanites are the most enriched in all the REE respect to alkali basalts, but all samples show

a general enrichment in light to medium rare earth elements (L-MREE) and slightly depletion in heavy rare-earth elements (HREE). Basanites show higher LREE/HREE, MREE/HREE ratios respect to alkali basalts.

Mantle-normalized incompatible element patterns (Fig. 3F; McDonough et al., 1992) of basanites from the Toprakkale volcanic field, are bell-shaped and similar to OIB compositions. They show enrichment in high-field-strength elements (HFSE) with positive anomalies of Zr, Nb, Ti and Ta, whereas the large ion lithophile elements (LILE) are characterized by slightly positive spike of Sr anomalies of K and Rb at variable extents. The alkaline basalts from both the Toprakkale area and the Amik Basin are characterized by flatter pattern to the respect of the basanites, with variable Nb, Ta and Ti anomalies and mainly positive LILE anomalies, similar to the enriched MORB compositions. All samples show also variable (from

Table 4
Chemical and isotope composition of noble-gases in fluid inclusions hosted in olivine (Ol) in selected samples of basalts and basanites.

Rocks	Sample	Min.	Analysis Date	[He] mol/g	[Ne] mol/g	⁴⁰ Ar mol/g	³⁶ Ar mol/g	⁴⁰ Ar* mol/g	⁴ He/ ⁴⁰ Ar*	⁴ He/ ²⁰ Ne	R/Ra	Rc/Ra	error +/-	⁴⁰ Ar/ ³⁶ Ar	Err (%)
BASANITES	R21	Ol	2014-10-28	4.27E-12	2.95E-15	2.69E-12	3.30E-15	1.72E-12	2.5	1449.6	7.31	7.32	0.05	815.8	0.06
	R25	Ol	2014-11-03	1.26E-11	1.01E-14	8.43E-12	1.36E-14	4.40E-12	2.9	1248.1	7.79	7.79	0.08	618.2	0.12
	R36	Ol	2014-10-28	3.11E-13	1.88E-15	8.46E-13	1.81E-15	3.11E-13	1.0	165.4	7.28	7.29	0.07	467.6	0.08
	R38	Ol	2014-10-27	7.83E-13	1.83E-16	1.25E-12	1.28E-15	8.70E-13	0.9	4281.2	7.48	7.48	0.07	974.9	0.18
	R48	Ol	2015-03-17	7.28E-13	6.08E-16	9.43E-13	1.56E-15	4.82E-13	1.5	1198.4	8.02	8.03	0.12	604.5	0.34
BASALTS	R32	Ol	2014-10-27	3.19E-13	1.00E-14	5.14E-12	1.51E-14	6.74E-13	0.5	31.8	7.55	7.62	0.09	340.1	0.04
	R40	Ol	2014-10-27	3.38E-13	4.11E-16	1.98E-12	4.25E-15	7.23E-13	0.5	823.5	7.52	7.53	0.15	465.7	0.13
	R41	Ol	2015-06-25	2.90E-13	2.37E-16	1.53E-12	2.29E-15	8.49E-13	0.3	1220.2	7.49	7.50	0.16	666.1	0.11
	R43	Ol	2015-03-17	8.15E-13	1.34E-16	1.03E-12	9.52E-16	7.45E-13	1.1	6080.5	7.85	7.85	0.15	1078.7	0.50
	R46	Ol	2015-03-16	1.98E-13	6.58E-16	1.01E-12	1.84E-15	4.65E-13	0.4	301.1	7.96	7.97	0.23	549.0	0.41

positive to negative) Pb spikes.

4.3. Noble gases

Nine analyses of He, Ne, Ar concentrations and ³He/⁴He, ⁴He/²⁰Ne, ⁴⁰Ar/³⁶Ar ratios have been carried out on accurately selected olivine crystals from some of the collected volcanics (Table 4).

Differences in the abundances (reported in mol/g) and isotope ratios of He, Ne and Ar between mantle-originated fluids and atmosphere can be used to determine whether air has been introduced into the samples. In particular, the ⁴He/²⁰Ne and ⁴⁰Ar/³⁶Ar ratios are the most-sensitive tracers of atmospheric contamination. The ⁴He/²⁰Ne ratio recorded in the samples ranges between 32 and 6080, with a mean of 1730, and makes negligible the correction of helium isotope ratio for atmospheric contamination (Table 4). Coherently, also the ⁴⁰Ar/³⁶Ar ratio displays values much higher than the atmospheric values ranging from 340 to 1078, with a mean of 657 (Table 4). In any case, as normally used in noble gas studies, we corrected the ³He/⁴He ratios based on the ⁴He/²⁰Ne ratio (e.g., Sano & Wakita, 1985) as follows:

$$R_c/R_a = [(R_M/R_a)(He/Ne)_M - (He/Ne)_A] / [(He/Ne)_M - (He/Ne)_A]$$

The ⁴⁰Ar concentration was corrected using the assumption that all ³⁶Ar is atmospheric, yielding the air-corrected ⁴⁰Ar* as

$$^{40}Ar^* = ^{40}Ar_m - ^{40}Ar_a \text{ with } ^{40}Ar_a = ^{36}Ar_m \cdot (^{40}Ar/^{36}Ar)_a$$

where ⁴⁰Ar_m and ³⁶Ar_m are the measured concentration of argon in the sample and ⁴⁰Ar_a that atmospheric-derived.

Fig. 4 confirms that despite He concentration of the data set varies by about two orders of magnitude, the ³He/⁴He ratio results rather constant, in the range previously reported (7–8 Ra). The absence of any clear trend in this plot excludes the occurrence of post-eruptive processes like addition of non-magmatic radiogenic ⁴He or cosmogenic ³He. These components are typically detected in those samples that are most depleted of He and consequently more prone to variations of their original ³He/⁴He value (Dunai and Baur, 1995; Hilton et al., 1995; Gautheron et al., 2005). In addition, we point out that the investigated rocks are sufficiently young (from 1.5 to 0.05 Ma) to exclude diffusion of ³He and ⁴He from the crystal lattice to the fluid inclusions at surface temperatures, as already suggested by Day et al. (2015). Finally, our analyses employed single-step crushing, a procedure that is known to minimize the release of matrix-sited components (e.g., Hilton et al., 1993, 2002).

For these reasons, post-eruptive secondary processes on noble gases may be neglected and data collected may be attributed to the parent magma.

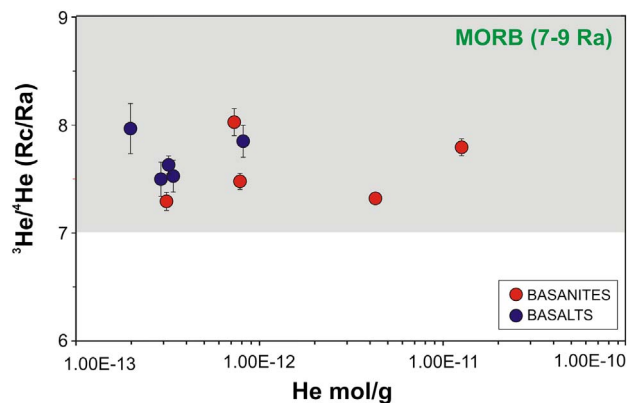


Fig. 4. Plot of ³He/⁴He (in Rc/Ra) versus He abundance in mol/g from fluid inclusions hosted in olivines separated from the investigated rocks. The Rc/Ra values are corrected for air contamination following the procedure described in the text. Vertical bars show the analytical errors.

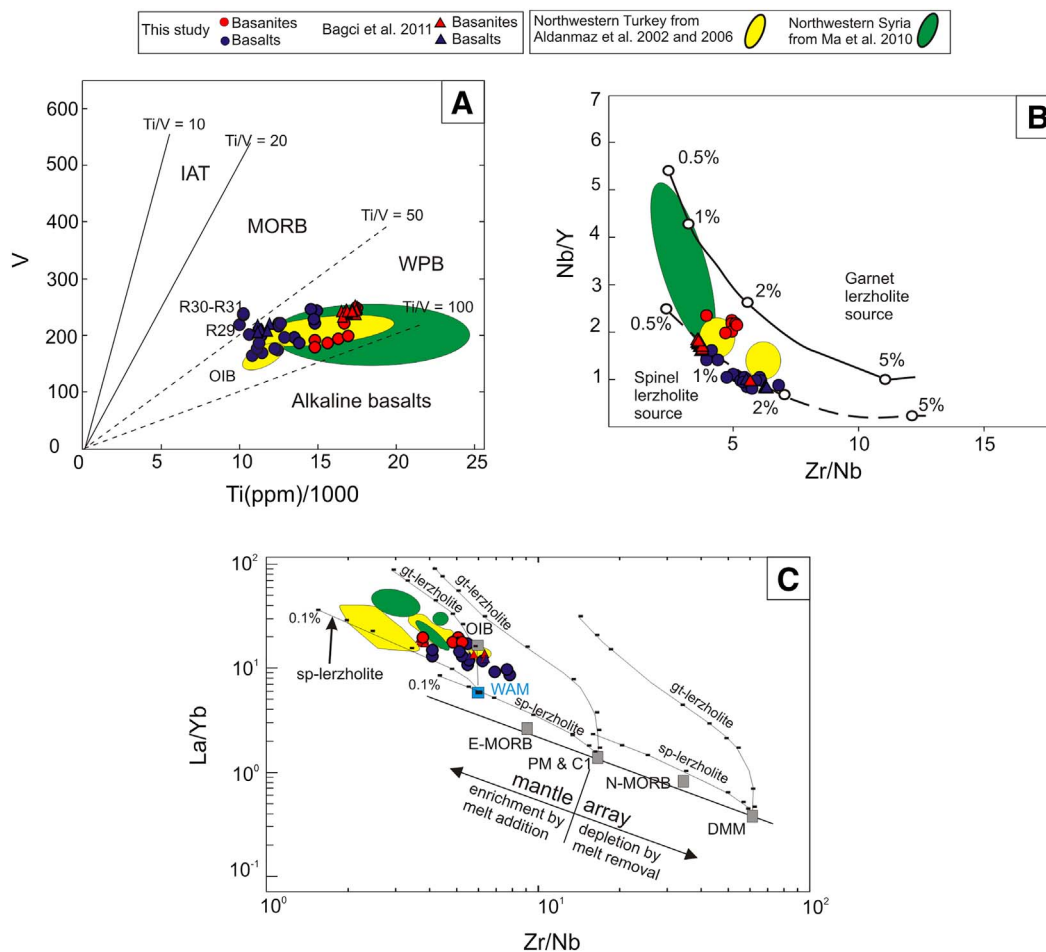


Fig. 5. A) Ti/1000 vs V discrimination diagrams after (Shervais, 1982), IAT – Island Arc tholeiite; MORB – Mid Ocean Ridge Basalts; WPB – Within plate basalts; OIB – Ocean Island Basalts; B) Zr/Nb vs Nb/Y discrimination diagrams (after Harangi, 2001); C) Zr/Nb vs La/Yb plot showing melt curves for garnet- and spinel-lherzolite magma sources (after Aldanmaz et al., 2006), WAM: Western Anatolian Mantle. Symbols as in Fig. 3. Data after Bagci et al. (2011), Ma et al. (2011) and Aldanmaz et al. (2006) are plotted for comparison.

5. Discussion

5.1. Petrological and geochemical features

The studied rocks from the Toprakkale volcanic field and the Amik Basin represents the products of a basic volcanism generated by decompressional melting under conditions of transtensional tectonic regime. The petrography and mineral chemistry of the identified alkali basalts and basanites from the two volcanic areas points out how these rocks underwent a rapid emplacement and cooling. The poor zoned olivine crystals, the small to medium size of the new formed phenocrysts, their quenching skeletal morphologies, showed also by oxide in the groundmass, are all features testifying the fast magma upraise and the rapid crystallization. In addition, the occurrence of relict olivine and clinopyroxene crystals, clinopyroxenite enclaves and large olivine/Cr-bearing spinel xenoliths (Fig. 2F), can be suggest a provenance of the parental magmas from the upper mantle or the lithosphere.

The geochemical features of the analysed rocks show patterns characterized by overall enrichment in HFSE, LREE and a slight HREE depletion and variable amount of LILE relative to primordial mantle composition. Basanites from Toprakkale volcanic field show bell-shape pattern (Fig. 5F, spider diagram) similar to Ocean Island Basalt (OIB), with slightly positive Nb, Ta and other HFS element anomalies (Weaver, 1991). The pattern of the alkaline basalts is flatter than the basanites showing a progressive depletion in all the incompatible elements and resembling an enriched-MORB compositions.

Further geochemical signatures, e.g. the Ti–V discrimination diagram (Fig. 5A), highlight the intraplate nature of all the studied rocks,

suggesting a general composition similar to other low-silica OIB-like volcanics from the Osmaniye Region (Bagci et al., 2011), from the Western Anatolian plate (Aldanmaz, 2002; Aldanmaz et al., 2006); and of the Arabian plate (Ma et al., 2011). Only the R29, R30 and R31 alkaline basalts from the Toprakkale area, marked by the lowest Ti/V ratios (< 50), fall in the MORB-type field.

The Zr/Nb vs Nb/Y diagram (Fig. 5B; Harangi, 2001), that discriminates between garnet and spinel lherzolite sources, shows how the samples including R36, R37 and R38 basanites (Toprakkale volcanic field) as well as alkaline basalts from either Toprakkale and Amik areas could be the result of 0.8–2% partial melting of a spinel lherzolite source. Conversely, the other basanites (R21, R22, R23, R25, R26, R28, R48) from the Toprakkale volcanic field taken out of the Amik Basin to the north could derive from a deeper magma source, intermediate between spinel and garnet lherzolite fields in agreement with the former results of Bagci et al. (2011). On the same diagram, the volcanics from NW Turkey and Syria generally follow the trend of the studied rocks, with only a small group of basanites from the NW Turkey that come from a deeper magma source. To constrain the depth range where partial melting occurred, we considered the maximum pressure limit of plagioclase-bearing lherzolite (Green and Hibberson, 1970; Obata, 1976; Herzeberg, 1978; O'Neill, 1981; Gasparik, 1984, 1987) together with the minimum pressure limit for the appearance of garnet calculated from spinel compositions (Webb and Wood, 1986). The range of equilibrium pressures overlaps the spinel stability field, namely between 1.0 and 2.2 GPa (e.g., Webb and Wood, 1986), corresponding to depths of 30 and 60 km for R36, R37, R38 basanites and all the alkali basalts, and depth of about 80 km for the other

basanites (R21, R22, R23, R25, R26, R28, R48).

The La/Yb vs Zr/Nb graph of Fig. 5C plots our data on literature melt curves for garnet- and spinel-lherzolite magma sources (Aldanmaz et al., 2006). The data are consistent with an origin from different partial melting degrees of an almost deep (> 30 km) compositionally distinct lherzolite source. Since our results well match with the previous information gained either for the Miocene to Quaternary intraplate volcanism of Anatolian plate in NW Turkey or for the West Anatolian Mantle (WAM) (Aldanmaz et al., 2006), we propose compositionally very similar mantle underlying the above-mentioned areas.

Enrichment of highly incompatible trace elements and LREE, and strong LREE/HREE fractionation can be explained either by moderate partial melting degrees of an enriched source or, alternatively, by lower melting degrees of a depleted source (Wilson and Downes, 2006). As stated previously, silica-undersaturated alkaline magmas, like the basanites and alkali basalts included in our samples suite, are normally related to relatively high pressure and small melting volumes of a garnet and spinel-garnet lherzolite source (Kushiro, 1996). Alkaline magmas with low silica contents can be produced by melting of both garnet lherzolite and pyroxenite (Keshav et al., 2004; Walter, 1998). Nearly all, high LREE/HREE ratios (e.g., La/Yb) of the studied lavas suggest that they were produced by low melting fraction of a garnet and spinel-garnet-bearing source. As suggested by Blundy et al. (1998), MREE/HREE ratios are even better proxies for garnet melting, where $(\text{Tb}/\text{Yb})_N < 1.06$ indicate melts derived from a spinel lherzolite source, while ratios > 1.06 characterize melts from a garnet lherzolite source. The measured $(\text{Tb}/\text{Yb})_N$ ranging from 1.45 to 2.25 indicating a lherzolite source that also fits with the lower SiO_2 and higher CaO and TiO_2 concentrations in the basanites compared to the alkali basalts. Moreover, the trace element abundances, further indicate very small partial melting degrees at greater depths than the alkali basalts (Hirose and Kushiro, 1993). The results point to an origin of the involved mafic melts from a predominantly spinel and garnet plus spinel stability zone.

Taking into account the variability of trace elements compositions (HFSE, LILE) and the LREE enrichment shown by the two groups of samples, we propose that metasomatic process related to the early subduction events, can represent the possible mechanisms explaining the more enriched compositions of basanites and the variability of the alkali basalts in agreement with the hypothesis of authors that previous study volcanism in these areas.

The LREE and HFSE (Ti) enriched volcanics studied here, could reflect derivation from an enriched MORB or OIB-like source. Several authors have suggested an origin for similar OIB-like magma component from recycled oceanic crust, which is likely to be present in the mantle as garnet pyroxenite and occurs as garnet pyroxenite layers within depleted (MORB-type) peridotite. The founding of partially resorbed amphibole xenocrysts in the basanite sample R25 (Kaersutite; brown hornblende) strengthens the hypothesis of a process related to the presence of “amphibole-rich metasomatic veins” as proposed by Pilet et al. (2008, 2010, 2011) to explain the origin of sodic alkaline mafic and ultrabasic-basic rocks (e.g., basanitic) erupted in intracrustal settings enriched in incompatible elements. This hypothesis was also taken into account by Bağcı et al. (2011), Aldanmaz et al. (2006), and Ma et al. (2011) to explain the origin of the Miocene-Quaternary intraplate alkaline rocks from the Osmaniye Region, the NW Turkey and NW Syria respectively. This mechanism would account for the geochemical differences, in terms of trace element abundances and their ratios as well as the noble gas geochemistry of fluid inclusions in olivines from the Amik and Toprakkale rocks.

The geochemical investigations are still ongoing and we argue that a Sr-Nd-Pb systematics may provide additional information to better constrain the origin, interactions and melting processes across the Arabian, Anatolian and African plates.

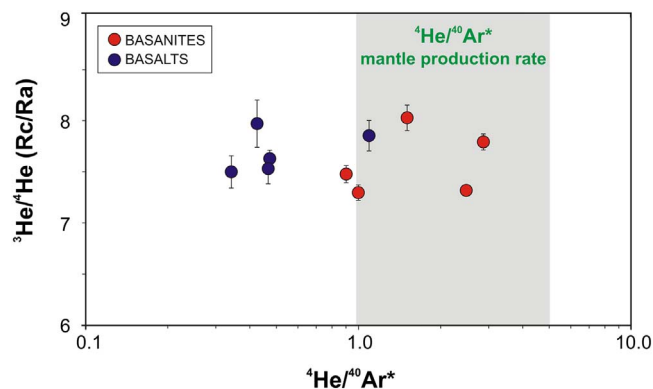


Fig. 6. Plot of $^4\text{He}/^{40}\text{Ar}^*$ versus $^3\text{He}/^4\text{He}$ corrected for atmospheric contamination (Rc/Ra) in fluid inclusions from olivines. Vertical bars show the analytical errors.

5.2. Noble gases in fluid inclusions

The volatiles extracted from selected rock samples, including basalts and basanites, display a range of $^4\text{He}/^{40}\text{Ar}^*$ between 0.4 and 3 (Fig. 6) mostly overlapping the typical production rate in mantle rocks (1.6–4.2, Graham, 2002). The $^4\text{He}/^{40}\text{Ar}^*$ of the basaltic samples are slightly lower than the production rate (0.4–1.1) (Fig. 6). These low values can be interpreted as the results of slightly higher degrees of mantle partial melting (e.g., Correale et al., 2016). Nevertheless, the simplest interpretation points toward the entrapment of a volatile phase released in the early stages of degassing, when the lower Ar solubility with respect to He (by a factor of about 10 in basalt melt, Jambon et al., 1986) causes the first gases to be enriched in Ar relatively to helium. Values within the production rate would sample a more degassed gas phase, with $^4\text{He}/^{40}\text{Ar}^*$ similar to those initially dissolved in the melt. The consistency of the measured ratios with those characteristic of production rate suggests that He and Ar degassed from magma in a closed system, thus limiting the possible range of He/Ar fractionation (Carroll and Webster, 1994). (See Fig. 7.)

Apart from this eventual and slightly different history of gas entrapment into fluid inclusions, the basanites and basalts appear

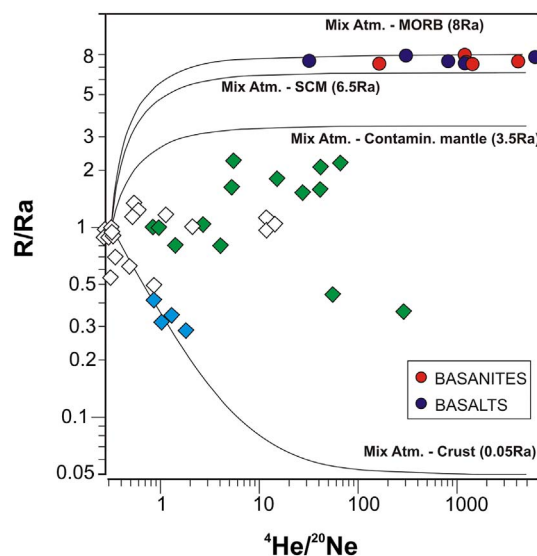


Fig. 7. Isotopic composition of helium extracted from olivines in basanites (red filled circles) and basalts (dark blue filled circles). Data from gas samples are reported for comparison: green filled diamonds: gases from DSF (Torstein et al., 2013); open diamonds: helium dissolved in shallow groundwaters from Amik Basin (after Yuce et al., 2014); light blue-filled diamonds: helium from deep Amik Basin groundwaters (after Yuce et al., 2014). (For interpretation of the references to colour in this figure legend, the reader is referred to the web version of this article.)

genetically comparable, as helium isotopes illustrate (Fig. 4). Indeed, the $^3\text{He}/^4\text{He}$ ratio measured in basalts and basanites results rather constant in the range 7.3–8 Ra, which implies the presence of a homogenous helium isotope signature in the mantle source beneath the “Karasu Rift”. Such values are commonly recorded in MORB reservoirs (usually stated between 7 and 9 Ra; e.g., Graham, 2002), collecting the upper convective asthenospheric mantle, and fall in the upper part of the range recently proposed for Continental Lithosphere (6.1 ± 2.1 Ra), where this range is referred to average ± 1 sigma of olivine measured by crushing (Day et al., 2015).

The combination of the major and trace elements geochemistry of bulk rocks with the He isotope composition of fluid inclusions from the same suite of samples allows better constraining the magma generation process. In contrast to the differences in major elements composition, the measured helium isotopes display no significant differences between basanites and basalts from the two Basins, indicating that those rocks produced by different partial melting degrees, experienced analogous processes affecting the helium systematic. The absence of helium isotope fractionation during magma generation justifies why clear variations of $^3\text{He}/^4\text{He}$ are not recorded between samples derived from different degrees of mantle melting.

The metasomatism highlighted by trace and incompatible elements geochemistry of the two rock suites is in agreement with results already gained by previous works although the noble gas geochemistry rules out major interactions with crust-originated fluids during transport and residence into the crust. Thus, processes like differential continental crust contamination can be excluded. Different hypotheses may exist to explain why helium isotopes are apparently not affected by the metasomatic enrichment that conversely is suggested by trace elements geochemistry. One possibility is that enrichment occurred recently, impeding significant ^4He production by U–Th decay in the mantle source of the lavas that in this way maintained its $^3\text{He}/^4\text{He}$ ratio. Besides, given the range of upper convective mantle (intended as MORB, normally indicated with 8 ± 1 Ra) and assuming that the starting value was between 8 and 9 Ra, we can also imagine that a certain amount of radiogenic decay related to metasomatism occurred and lowered the values to the observed range (7.3–8 Ra). Such possibilities remain now unconstrained. The ophiolitic nappes and crustal products covering the Amik Basin and the Toprakkale volcanic district did not produce any contamination of the volcanics, moreover the volcanic activity over different tectonic plates (e.g., Arabian and Anatolian) exhibits similar geochemical features and denotes the occurrence of very similar melting, uprising and metasomatic processes.

As a final comment, we argue that although the volcanic activity in the both the Amik and Toprakkale Basins developed over ~ 2 Ma, as shown by the K–Ar dating, relatively low magma volumes had been produced and built up the present-day small volcanic edifices. The production of small magma batches implies that the ongoing active degassing of volcanic-type volatiles as detected over the Amik Basin (Yuce et al., 2014), cannot be related to the volcanism, but to the degassing through the various splays of the DSF in agreement with the results gained along the DSF by Torfstein et al. (2013), about 300 km southward. The measured $^3\text{He}/^4\text{He}$ ratios of 6.6 ± 0.7 Ra (in olivines and diopside crystals), clash with the helium isotope signature of fluids vented over the same area displaying a maximum value of 2 Ra. The studies of Yuce et al. (2014) and Torfstein et al. (2013) confirm that magmatic helium in gas and water samples is heavily diluted by crustal-radiogenic helium during the rising or residence in the crust, and therefore, measurements developed in mafic crystals of volcanic rocks are crucial to correctly interpret the significance of the values measured in currently emitted fluids highlighting the absence of ongoing active degassing.

6. Conclusions

Magmas emplacements over the Amik and Toprakkale-Erzin areas

(SE Turkey) located between the Anatolian, Arabian and African tectonic plates were triggered by discontinuities generated by the strike-slip Dead Sea and the East Anatolian lithospheric fractures. There is a general agreement based on the petrology, geochemistry and K–Ar dating that the alkali olivine basalts and the basanites derived from asthenospheric mantle sources.

The combined results of noble gas geochemistry of the fluid inclusions in olivines as well as the geochemical and mineralogical-petrographic features of the volcanic rocks, allow to gain a better insight into the genesis and the process behind the magmas generation.

Our results, as well as former studies carried out on the petrology, geochemistry and K–Ar dating of the basaltic volcanics within these zones (Çapan et al., 1987; Polat et al., 1997; Parlak et al., 1997, 1998, 2000; Arger et al., 2000; Yurtmen et al., 2000, 2002; Alici et al., 2001; Rojay et al., 2001; Bağcı et al., 2011), coherently suggest that volcanics in this region were derived from an OIB-type mantle source variously enriched by metasomatic fluid. At various times, the lithospheric fractures formed by the strike-slip DSF and the EAF triggered the magma ascent in correspondence to extensional or transtensional faults that acted as conduits.

The variability of the high LREE/MREE ratios indicates that the degree of mantle partial melting has spatially and temporally changed. The analysed rocks indicate mantle melting at different depths with two mantle horizons recognized as a deeper spinel lherzolite source and an intermediate one between spinel and garnet lherzolite. Petrologic considerations constrain such mantle sources in a depth range between 30 and 80 km, while trace elements suggest the possible occurrence of metasomatic processes.

The $^3\text{He}/^4\text{He}$ measured in fluid inclusions of a selected suite of olivines fall in the range of 7.3–8.0 Ra denoting rather homogeneous values across the vertical mantle section sampled by the studied lavas. The recorded helium isotope ratios are fully in the range of MORB values ruling out significant crustal contaminations or assimilation suffered by the parental mantle. Bringing together the results of the noble gas isotopes in fluid inclusions and the bulk rock geochemistry of the same suite of samples, we propose that small volumes of alkaline magmas over the Amik Basin and Toprakkale-Erzin areas, have been produced by variable degrees of partial melting of an originally depleted mantle source probably metasomatized by amphibole-rich veins (Niu, 2008; Pilet et al., 2011) or recycled oceanic crust during the ascent through lithosphere. Further combined studies, including lithophile elements isotopes, are needed to gain a better insight on the mantle metasomatism processes across the three convergent plate tectonics. Constrains might be highlighted by the contemporary analysis of the solid and fluid phases of the same rocky sample have to be carried out on the volcanics outcropping around the junction area of the Eurasian, African and Anatolian plates.

Acknowledgments

This work has been funded by the Scientific and Technological Research Council of Turkey (TUBITAK) with the project (COST) n° 111Y090. The authors wish to thank Mariano Tantilillo for the valuable support in noble gas analyses. We would like to extend our thanks for Prof. Dr. Musa Alpaslan who provided some rock samples and their chemical results. We finally thank two anonymous reviewers for their helpful reviews, which strongly improved the manuscript.

References

- Aldanmaz, E., 2002. Mantle source characteristics of alkali basalts and basanites in an extensional intracontinental plate setting, western Anatolia, Turkey: implications for multi-stage melting. *Int. Geol. Rev.* 44, 440–457.
- Aldanmaz, E., Koprubasi, N., Gurer, Ö.F., Kaymakci, N., Gourgaud, A., 2006. Geochemical constraints on the Cenozoic, OIB-type alkaline volcanic rocks of NW Turkey: implications for mantle sources and melting processes. *Lithos* 86, 50–76.
- Alici, P., Temel, A., Gourgaud, A., Vidal, P., Gündoğdu, M.N., 2001. Quaternary tholeiitic

- to alkaline volcanism in the Karasu Valley, Dead Sea rift zone, southeast Turkey: Sr-Nd-Pb-O isotopic and trace-element approaches to crust-mantle interaction. *Int. Geol. Rev.* 43, 120–138.
- Arger, J., Mitchell, J., Waterway, R.W.C., 2000. Neogene and Quaternary volcanism of SE Turkey. In: Bozkurt, E., Winchester, J.A., Piper, J.D.A. (Eds.), *Tectonics and Magmatism in Turkey and the Surrounding Area*. 173. Geological Society, London, Special Publications, pp. 459–487.
- Bagci, U., Alpaslan, M., Frei, R., Ma, Kurt, Temel, A., 2011. Different degrees of partial melting of the enriched mantle source for Plio – Quaternary basic volcanism, Toprakçale (Osmaniye) region, southern Turkey. *Turk. J. Earth Sci.* 20, 115–135. <http://dx.doi.org/10.3906/Yer-1003-30>.
- Barka, A., Reilinger, R., 1997. Active tectonics of the Mediterranean region: deduced from GPS, neotectonic and seismicity data. *Ann. Geofis.* XI (3), 587–610.
- Blundy, J., Robinson, J.A.C., Wood, B., 1998. Heavy REE are compatible in clinopyroxene from the spinel lherzolite solidus. *Earth Planet. Sci. Lett.* 160, 493–504.
- Boynton, W.V., 1985. Cosmochemistry of the rare earth elements: Meteorite studies. In: Henderson, P. (Ed.), *Rare Earth Element Geochemistry*. Elsevier, Amsterdam, pp. 115–1522. *Developments in Geochemistry* 2.
- Çapan, U.Z., Vidal, P., Cantagrel, J.M., 1987. K-Ar, Nd, Sr and Pb isotopic study of the Quaternary volcanism in Karasu Rift (Hatay), N-end of Dead Sea rift zone in SE Turkey. *H.Ü. Yerbilimleri* 14, 165–178.
- Carroll, M. R., & Webster, J. D. (1994). Sulfur, noble gases, and halogens: solubility relations of the less abundant volatile species in magmas. In M. R. Carroll, & J. R. Holloway (Eds.), *Reviews in Mineralogy*, V30. (pp. 331–371). (Mineralogical Society of America).
- Correale, A., Rizzo, A.L., Barry, P.H., Lu, J., Zheng, J., 2016. Refertilization of lithospheric mantle beneath the Yangtze craton in South-East China: evidence from noble gases geochemistry. *Gondwana Res.* 38, 289–303. <http://dx.doi.org/10.1016/j.gr.2016.01.003>.
- Day, J.M.D., Barry, P.H., Hilton, D.R., Burgess, R., Graham-Pearson, D., Taylor, L.A., 2015. The helium flux from the continents and ubiquity of low-³He/⁴He recycled crust and lithosphere. *Geochim. Cosmochim. Acta* 153, 116–133.
- Di Piazza, A., Rizzo, A.L., Barberi, F., Carapezza, M.L., De Astis, G., Romano, C., Sortino, F., 2015. Geochemistry of the mantle source and magma feeding system beneath Turrialba Volcano, Costa Rica. *Lithos* 232, 319–335.
- Dunai, T.J., Baur, H., 1995. Helium, neon, and argon systematics of the European subcontinental mantle: implications for its geochemical evolution. *Geochim. Cosmochim. Acta* 59, 2767–2783.
- Gasparik, T., 1984. Experimental study of subsolidus phase relations and mixing properties of pyroxene in the system CaO-Al₂O₃-SiO₂. *Contrib. Mineral. Petrol.* 85, 186–196.
- Gasparik, T., 1987. Ortho-pyroxene thermobarometry in simple and complex systems. *Contrib. Mineral. Petrol.* 96, 357–370.
- Gautheron, C., Moreira, M., Allègre, C., 2005. He, Ne and Ar composition of the European lithospheric mantle. *Chem. Geol.* 217, 97–112.
- Graham, D.W., 2002. Noble gas isotope geochemistry of mid-oceanic ridge and ocean island basalts: characterization of mantle source reservoirs. In: Porcelli, D.P., Ballentine, C.J., Wieler, R. (Eds.), *Noble Gases. Reviews in Mineralogy and Geochemistry*, vol. 47. pp. 247–317.
- Green, D.H., Hibberson, W., 1970. The instability of plagioclase in peridotite at high pressure. *Lithos* 3, 209–221.
- Gürsoy, H., Tatar, O., Piper, J.D.A., Heimann, A., Mesci, L., 2003. Neotectonic deformation linking the east Anatolian and Karataş-Osmaniye intracontinental transform fault zones in the Gulf of Iskenderun, southern Turkey, deduced from paleomagnetic study of the Ceyhan-Osmaniye volcanics. *Tectonics* 22 (6), 1–12.
- Harangi, S., 2001. Neogene magmatism in the Alpine-Pannonian Transition Zone - a model for melt generation in a complex geodynamic setting. *Acta Vulcanol.* 13, 25–39.
- Hampton, M.R., 1987. Constraints on Arabian plate motion and extensional history of the Red Sea. *Tectonics* 6, 687–705.
- Herzeberg, C.T., 1978. Pyroxene geothermometry and geobarometry: experimental and thermo-dynamic evaluation of some subsolidus phase relations involving pyroxenes in the system CaO-MgO-Al₂O₃-SiO₂. *Geochim. Cosmochim. Acta* 42, 945–958.
- Hilton, D.R., Hammerschmidt, K., Looch, G., Friedrichsen, H., 1993. Helium and argon isotope systematics of the central Lau basin and Valu Fa Ridge: evidence of crust/mantle interactions in a back-arc basin. *Geochim. Cosmochim. Acta* 57 (12), 2819–2841.
- Hilton, D.R., Barling, J., Wheller, G.E., 1995. Effect of shallow level contamination on the helium isotope systematics of ocean-island lavas. *Nature* 373, 330–333.
- Hilton, D.R., Fischer, T.P., Marty, B., 2002. Noble gases and volatile recycling at subduction zones. *Rev. Mineral. Geochem.* 47 (1), 319–370.
- Hirose, K., Kushiro, I., 1993. Partial melting of dry peridotites at high pressures: determinations of compositions of melt segregated from peridotites using aggregates of diamonds. *Earth Planet. Sci. Lett.* 114, 477–489.
- Jambon, A., Weber, H., Braun, O., 1986. He, Ne, Ar, Kr and Xe in a basalt melt in the range 1250–1600 °C. Geochemical implications. *Geochim. Cosmochim. Acta* 50, 401–408.
- Keshav, S., Gudfinsson, G.H., Sen, G., Fei, Y., 2004. High-pressure melting experiments on garnet clinopyroxene and the alkalic to tholeiitic transition in ocean-island basalts. *Earth Planet. Sci. Lett.* 223, 365–379.
- Kiratzi, A.A., 1993. A study of the active crustal deformation of the north and east Anatolian fault zones. *Tectonophysics* 225, 191–203.
- Kushiro, I., 1996. Partial melting of a fertile mantle peridotite at high pressures: an experimental study using aggregates of diamond. In: Basu, A., Hart, S.R. (Eds.), *Earth Processes: Reading the Isotopic Code*. AGU Monograph, vol. 95. pp. 109–122.
- Le Maitre, R.W., 2002. *Igneous Rocks: a Classification and Glossary of Terms*. Recommendations of the International Union of Geological Sciences Subcommission on the Systematics of Igneous Rocks. Cambridge University Press, Cambridge, pp. 236.
- Ma, G.S.K., Malpas, J., Xenophontos, C., Chan, G.H.N., 2011. Petrogenesis of latest Miocene-Quaternary continental intraplate volcanism along the northern Dead Sea fault system (Al Ghab-Homs Volcanic Field), western Syria: evidence for lithosphere-stenosphere interaction. *J. Petrol.* 52, 401–430.
- Mahmoud, Y., Masson, F., Meghraoui, M., Cakir, Z., Alchalbi, A., Yavasoglu, H., Yönlü, O., Daoud, M., Ergintav, S., Inan, S., 2013. Kinematic study at the junction of the east Anatolian fault and the Dead Sea fault from GPS measurements. *J. Geodyn.* 67, 30–39. <http://dx.doi.org/10.1016/j.jog.2012.05.006>.
- Martelli, M., Rizzo, A.L., Renzulli, A., Ridolfi, F., Arienzo, L., Rosciglione, A., 2014. Noble-gas signature of magmas from a heterogeneous mantle wedge: the case of Stromboli Volcano (Aeolian Islands, Italy). *Chem. Geol.* 368, 39–53. <http://dx.doi.org/10.1016/j.chemgeo.2014.01.003>.
- McClusky, S., Balassanian, A.A., Barka, C., Demir, S., Ergintav, I., Georgiev, O., Gürkan, M., Hamburger, K., Hurst, H.G., Kahle, K., Kastens, G., Kekelidze, R., King, V., Kotzev, O., Lenk, S., Mahmoud, A., Mishin, M., Nadariya, A., Ouzounis, D., Paradissis, Y., Peter, M., Prilepin, R.E., Reilinger, İ., Sanlı, H., Seeger, A., Tealeb, M.N., Toksöz, G., Veis, 2000. Global Positioning System constraints on plate kinematics and dynamics in the Eastern Mediterranean and Caucasus. *J. Geophys. Res.* 105, 5695–5720.
- McDonough, W.F., Sun, S.S., Ringwood, A.E., Jagoutz, E., Hofmann, A.W., 1992. K, Rb and Cs in the earth and moon and the evolution of the earth's mantle. *Geochim. Cosmochim. Acta* 56, 1001–1012.
- Meghraoui, M., Çakır, Z., Masson, F., Mahmood, Y., Ergintav, S., Alchalbi, A., Inan, S., Daoud, M., Yönlü, O., Altunel, E., 2011. Kinematic modelling at the triple junction between the Anatolian, Arabian, African plates (NW Syria and in SE Turkey). *Geophys. Res. Abstr.* 13, EGU2011-EG12599.
- Muehlberger, R.W., 1981. The splintering of the Dead Sea fault zone in Turkey H. U. *Yerbilimleri Bull.* 8, 123–130.
- Niu, Y., 2008. The origin of alkaline lavas. *Science* 320, 883–884.
- Obata, M., 1976. The solubility of Al₂O₃ in orthopyroxenes, in spinel and plagioclase peridotites and spinel pyroxenites. *Am. Mineral.* 61, 804–816.
- O'Neill, C., 1981. The transition between spinel lherzolite and garnet lherzolite, and its use as a geobarometer. *Contrib. Mineral. Petrol.* 77, 185–194.
- Parlak, O., Kozlu, H., Demirkol, C., Delaloye, M., 1997. Intracontinental Plio-Quaternary volcanism along the African-anatolian plate boundary, southern Turkey. *Ofoliti* 22, 111–117.
- Parlak, O., Kop, A., Ünügenç, U.C., Demirkol, C., 1998. Geochemistry and geochronology of basaltic rocks in the Karasu graben around Kırıkhan (Hatay), southern Turkey. *Turk. J. Earth Sci.* 7, 53–61.
- Parlak, O., Delaloye, M., Kozlu, H., Fontignie, D., 2000. Trace element and Sr-Nd isotope geochemistry of the alkali basalts observed along the Yumurtalık Fault (Adana) in southern Turkey. *Yerbilimleri* 22, 137–148.
- Pilet, S., Baker, M.B., Stolper, E.M., 2008. Metasomatized lithosphere and the origin of alkaline lavas. *Science* 320, 916–919.
- Pilet, S., Ulmer, P., Villiger, S., 2010. Liquid line of descent of a basaltic liquid at 1.5 GPa: constraints on the formation of metasomatic veins. *Contrib. Mineral. Petrol.* 159, 621–643.
- Pilet, S., Baker, M.B., Othmar, M. & Stolper, E. M., 2011. Monte Carlo simulations of metasomatic enrichment in the lithosphere and implications for the source of alkaline basalts. *J. Petrol.* 52 (7–8), 1415–1442. <http://dx.doi.org/10.1093/ptrology/egr007>.
- Polat, A., Kerrich, R., Casey, J.F., 1997. Geochemistry of Quaternary basalts erupted along the east Anatolian and Dead Sea fault zones of southern Turkey: implications for mantle sources. *Lithos* 40, 55–68.
- Pouchou, J.L., Pichoir, L., 1985. Les éléments très légers en microanalyse X – possibilités des modèles récents de quantification. *J. Microsc. Spectrosc. Electron.* 11, 229–250.
- Pouchou, J.L., Pichoir, L., 1984. Possibilités d'analyse en profondeur à la microsonde électronique. *J. Microsc. Spectrosc. Electron.* 9, 99–100.
- Reilinger, R., McClusky, S.C., Oral, M.B., King, W., Toksöz, M.N., 1997. Global positioning, system measurements of present-day crustal movements in the Arabia-Africa-Eurasia plate collision zone. *J. Geophys. Res.* 102, 9983–9999.
- Rizzo, A., Barberi, F., Carapezza, M.L., Di Piazza, A., Francalanci, L., Sortino, F., D'Alessandro, W., 2015. New mafic magma refilling a quiescent volcano: evidence from He-Ne-Ar isotopes during the 2011–2012 unrest at Santorini, Greece. *Geochim. Geophys. Geosyst.* <http://dx.doi.org/10.1002/2014GC005653>.
- Rojay, B., Heimann, A., Toprak, V., 2001. Neotectonic and volcanic characteristics of the Karasu fault zone (Anatolia, Turkey): the transition zone between the Dead Sea transform and the east Anatolian fault zone. *Geodin. Acta* 14, 197–212.
- Sano, Y., Wakita, H., 1985. Geographical distribution of ³He/⁴He ratios in Japan: implications for arc tectonics and incipient magmatism. *J. Geophys. Res. Solid Earth* 90, 8729–8741. (1978–2012). <http://dx.doi.org/10.1029/JB090iB10p08729>.
- Şengör, A.M.C., N. Görür, F. Şaroğlu, (1985). Strike-slip faulting and related basin formation in zones of tectonic escape: Turkey as a case study, in: K. Biddle, N. Christie-Blick (Eds), *Strike-slip Deformation, Basin Formation and Sedimentation*. Society of Economic Paleontologists and Mineralogists, Special Publications 37, 227–264.
- Shervais, J.W., 1982. Ti–V plots and the petrogenesis of modern ophiolitic lavas. *Earth Planet. Sci. Lett.* 59, 101–118.
- Stormer, J.C., 1973. Calcium zoning in olivine and its relationship to silica activity and pressure. *Geochim. Cosmochim. Acta* 37, 1815–1821.
- Sun, S., McDonough, W.F., 1989. Chemical and isotopic systematics of oceanic basalts: implications for mantle composition and processes. In: Saunders, A.D., Norry, M.J. (Eds.), *Magmatism in Ocean Basins*. 42. Geological Society London Special Publications, pp. 313–345.

- Torfstein, A., Hammerschmidt, K., Friedrichsen, H., Starinsky, A., Garfunkel, Z., Kolodny, Y., 2013. Helium isotopes in Dead Sea transform waters. *Chem. Geol.* 352, 188–201. <http://dx.doi.org/10.1016/j.chemgeo.2013.06.008>.
- Walter, M.J., 1998. Melting of garnet peridotite and the origin of komatiite and depleted lithosphere. *J. Petrol.* 39 (1), 29–60.
- Weaver, B.L., 1991. The origin of ocean island end-member compositions: trace element and isotopic constraints. *Earth Planet. Sci. Lett.* 104, 381–397.
- Webb, S.A.C., Wood, B.J., 1986. Spinel-pyroxene-garnet relationships and their dependence on Cr/Al ratio. *Contrib. Mineral. Petrol.* 92, 471–480.
- Wilson, M., Downes, H., 2006. Tertiary-Quaternary intraplate magmatism in Europe and its relationship to mantle dynamics. In: Gee, D.G., Stephenson, R. (Eds.), *European Lithosphere Dynamics*. Geological Society of London Memoir 32 Geological Society of London, London, 978-1-86239-212-0, pp. 147–166.
- Yuce, G., Italiano, F., D'Alessandro, W., Yalcin, T.H., Yasin, D.U., Gulbay, A.H., Ozyurt, N.N., Rojaj, B., Karabacak, V., Bellomo, S., Brusca, L., Yang, T., Fu, C.C., Lai, C.W., Ozacar, A., Walia, V., 2014. Origin and interactions of fluids circulating over the Amik Basin (Hatay-Turkey) and relationships with the hydrologic, geologic and tectonic settings. *Chem. Geol.* 378–379, 75–88.
- Yurtmen, S., Rowbotham, G., İşler, F., Floyd, P.A., 2000. Petrogenesis of basalts from southern Turkey: the Plio-Quaternary volcanism to the north of Iskenderun Gulf. In: Bozkurt, E., Winchester, J.A., Piper, J.D.A. (Eds.), *Tectonics and Magmatism in Turkey and the Surrounding Area*. 173. Geological Society, London, Special Publications, pp. 489–512.
- Yurtmen, S., Guillou, H., Westaway, R., Rowbotham, G., Tatar, O., 2002. Rate of strike-slip motion on the Amanos Fault (Karasu Valley, southern Turkey) constrained by K–Ar dating and geochemical analysis of Quaternary basalts. *Tectonophysics* 344, 207–246.
- Yürür, M.T., Chorowicz, J., 1998. Recent volcanism, tectonics, and plate kinematics near the junction of the African, Arabian, and Anatolian plates. *J. Volcanol. Geotherm. Res.* 85, 1–15.